INTERNATIONAL JOURNAL FOR NUMERICAL METHODS IN ENGINEERING
Int. J. Numer. Meth. Engng 2005; **63**:709–736
Published online 9 March 2005 in Wiley InterScience (www.interscience.wiley.com). DOI: 10.1002/nme.1298

Influence functions and goal-oriented error estimation for finite element analysis of shell structures

Thomas Grätsch and Klaus-Jürgen Bathe*, †

Department of Mechanical Engineering, Massachusetts Institute of Technology, 77 Massachusetts Avenue, Cambridge, MA 02139, U.S.A.

SUMMARY

In this paper, we first present a consistent procedure to establish influence functions for the finite element analysis of shell structures, where the influence function can be for any linear quantity of engineering interest. We then design some goal-oriented error measures that take into account the cancellation effect of errors over the domain to overcome the issue of over-estimation. These error measures include the error due to the approximation in the geometry of the shell structure. In the calculation of the influence functions we also consider the asymptotic behaviour of shells as the thickness approaches zero. Although our procedures are general and can be applied to any shell formulation, we focus on MITC finite element shell discretizations. In our numerical results, influence functions are shown for some shell test problems, and the proposed goal-oriented error estimation procedure shows good effectivity indices. Copyright © 2005 John Wiley & Sons, Ltd.

KEY WORDS: shell structures; influence functions; goal-oriented error estimation; MITC shell elements

1. INTRODUCTION

In engineering design, finite element shell discretizations are used abundantly to analyse three-dimensional structures that are thin in one direction and long in the other two directions: For instance, in civil engineering, large roofs and wide-spanned bridges are commonly analysed using shell finite element models, and in mechanical engineering shell models are employed for the analysis of motor car bodies, airplane bodies and rockets (see e.g. Reference [1]).

Shell structures are difficult to analyse because of their complex physical behaviour. However, while shell analyses are abundantly performed, in engineering practice and research, the calculation of influence functions has largely not been pursued. And yet influence functions generally provide valuable insight into the load bearing capacity of a structure. Also, these

*Correspondence to: K. J. Bathe, Department of Mechanical Engineering, Massachusetts Institute of Technology, 77 Massachusetts Avenue, Cambridge, MA 02139, U.S.A.
†E-mail: kjb@mit.edu

Contract/grant sponsor: German Research Foundation (DFG); contract/grant number: GR 1894/2-1

Received 10 May 2004
Revised 8 November 2004
Accepted 8 December 2004

functions can be directly of value in the design of structures that need be analysed for a large number of load cases and in establishing error measures.

In this paper, we present a consistent procedure to establish influence functions for shell structures. The quantity of interest, for which we are seeking the influence function, can be any linear quantity of the solution space as for example the stresses integrated over a small area of the domain or the tractions integrated over a portion of the support boundary. We emphasize that the developed influence functions satisfy a so-called *consistency condition*. This condition asserts that the integration of the load multiplied by the influence function is equal to the value obtained in a finite element analysis evaluating the quantity of interest as usual. The presented procedure can be used with any shell finite element discretization scheme, but we demonstrate the method using MITC shell finite elements.

The asymptotic analysis of shell structures succinctly shows that with decreasing thickness, the behaviour of a shell generally converges to a specific limit state that is either membrane dominated, bending dominated, or of a mixed stress state [2, 3]. The classification of a shell problem depends on the geometry, the displacement boundary conditions and the load application. Since influence functions are independent of the actually applied load, they can provide important information on the stresses in specific regions of the shell, namely the influence of the load application and of the shell thickness.

We also extend in this paper the recently proposed goal-oriented error estimation procedures to the analysis of shell structures. These procedures allow to estimate the error in arbitrary quantities of interest. The key for employing these methods is the formulation of a dual problem that contains the information for an accurate error estimate in the quantity of interest. The solution of this dual problem is the influence function, so that once the influence function has been established, goal-oriented error measures can straightforwardly be obtained. The proposed goal-oriented error estimates also take into account the error due to the approximation in the geometry of the shell structure.

Related to our work is the research of Çirak and Ramm [4], Prudhomme *et al.* [5], Oden *et al.* [6], Bangerth and Rannacher [7], Becker and Rannacher [8] and Rannacher and Suttmeier [9], who also consider goal-oriented error estimation in the analysis of structures. In contrast to the work of Çirak and Ramm we detail our approach for the use in shell finite element analysis rather than focusing on 3D elasticity equations, and, also, we also use a consistent approach to calculate the influence functions for stress quantities. Of course, we focus on any stresses in our goal-oriented error estimate. In contrast to the work of Oden *et al.* we present error measures in which a genuine shell formulation is employed for the complete analysis process and do not use the shell displacement solution in 3D displacement-based elasticity equations for the error estimate. When considering thin shells, such approach must be expected to lead in general to errors due to the 'locking' phenomenon and hence to not accurately measure the actual error incurred [2, 3, 10, 11]. Another important point of our proposed error measure is that in contrast to the contributions [4–6] our approach also takes into account the cancellation effect of the error over the solution domain to address the issue of over-estimation that may occur when using energy norm estimates.

In the following sections, we first introduce the shell formulation used and briefly the MITC approach for the derivation of the influence functions. Then we comment on the asymptotic behaviour of shells. Next, we derive the calculation of influence functions and explicitly address the numerical implementation for MITC shell elements. The influence functions are the basic ingredients of the goal-oriented error estimation procedures, which we then present.

In our numerical examples we calculate some influence functions of shell test problems and we give some results using goal-oriented error estimation procedures. The solutions illustrate that the influence functions can also be very valuable in asymptotic studies of shell behaviour (as the thickness becomes very small). We find that the error measures obtained are remarkably accurate in the problems considered.

2. FORMULATION OF THE SHELL MODEL

In this section, we briefly recall the shell finite element discretization used. We closely follow the exposition given by Chapelle and Bathe [3].

2.1. Continuum mechanics-based shell models

We consider a linear elastic shell-like structure whose mid-surface, $\mathscr{S}$, is defined by a single chart $\boldsymbol{\phi}$, which is an injective mapping from ω into $\mathbb{R}^3$ such that $\mathscr{S}=\boldsymbol{\phi}(\overline{\omega})$, where ω denotes an open domain of $\mathbb{R}^2$ that is called the surface reference domain. Denoting by (ξ^1, ξ^2) the co-ordinates used in $\mathbb{R}^2$ we assume that $\boldsymbol{\phi}$ is such that the vectors

$$\mathbf{a}_\alpha = \frac{\partial \boldsymbol{\phi}(\xi^1, \xi^2)}{\partial \xi^\alpha}, \quad \alpha = 1, 2 \tag{1}$$

form the covariant basis for the tangential plane to the mid-surface at any point with co-ordinates in $\overline{\omega}$. Defining the unit normal vector of the surface by

$$\mathbf{a}_3 = \frac{\mathbf{a}_1 \times \mathbf{a}_2}{\|\mathbf{a}_1 \times \mathbf{a}_2\|} \tag{2}$$

we can introduce the 3D chart

$$\boldsymbol{\Phi}(\xi^1, \xi^2, \xi^3) = \boldsymbol{\phi}(\xi^1, \xi^2) + \xi^3 \mathbf{a}_3(\xi^1, \xi^2) \tag{3}$$

which maps the 3D reference domain defined by

$$\Omega = \left\{ (\xi^1, \xi^2, \xi^3) \in \mathbb{R}^3 \mid (\xi^1, \xi^2) \in \omega, \xi^3 \in \left]-\frac{t}{2}, +\frac{t}{2}\right[\right\} \tag{4}$$

into the 3D geometric domain, $\mathscr{B}$, such that $\mathscr{B}=\boldsymbol{\Phi}(\overline{\Omega})$ where t denotes the thickness of the shell. The boundary Γ of the domain Ω consists of two parts Γ_D and Γ_N such that $\Gamma = \overline{\Gamma_\mathrm{D} \cup \Gamma_\mathrm{N}}$ and $\Gamma_\mathrm{D} \cap \Gamma_\mathrm{N} = \emptyset$. For simplicity, we assume zero displacements on the Dirichlet part Γ_D and zero imposed tractions on the Neumann part Γ_N of the boundary. The displacement $\mathbf{U}=\mathbf{U}(\xi^1, \xi^2, \xi^3)$ satisfies the 3D variational formulation:

Find $\mathbf{U} \in V$ such that

$$A^{(3\mathrm{D})}(\mathbf{U}, \mathbf{V}) = F^{(3\mathrm{D})}(\mathbf{V}) \quad \forall \mathbf{V} \in V \tag{5}$$

where V denotes an appropriate functional space that takes into account the homogeneous boundary conditions on Γ_D. The symmetric and coercive bilinear form $A^{(3D)}(\mathbf{U}, \mathbf{V})$ and the linear functional $F^{(3D)}(\mathbf{V})$ of the dual space V' are

$$A^{(3D)}(\mathbf{U}, \mathbf{V}) = \int_\Omega H^{ijkl} e_{ij}(\mathbf{U}) e_{kl}(\mathbf{V}) \sqrt{g}\, d\xi^1\, d\xi^2\, d\xi^3 \tag{6}$$

$$F^{(3D)}(\mathbf{V}) = \int_\Omega \mathbf{F} \cdot \mathbf{V} \sqrt{g}\, d\xi^1\, d\xi^2\, d\xi^3 \tag{7}$$

where $\mathbf{F}$ represents body forces in 3D and $g = \det(\mathbf{g}_i \cdot \mathbf{g}_j)$ with the 3D covariant base vectors $\mathbf{g}_i = \partial \mathbf{\Phi} / \partial \xi^i$. The covariant Green–Lagrange strain tensor components are

$$e_{ij}(\mathbf{U}) = \tfrac{1}{2}(\mathbf{g}_i \cdot \mathbf{U}_{,j} + \mathbf{g}_j \cdot \mathbf{U}_{,i}) \tag{8}$$

and H^{ijkl} is the material tensor corresponding to Hooke's law

$$H^{ijkl} = \frac{Ev}{(1+v)(1-2v)} g^{ij} g^{kl} + \frac{E}{2(1+v)} (g^{ik} g^{jl} + g^{il} g^{jk}) \tag{9}$$

in which E and v denote Young's modulus and Poisson's ratio, respectively.

We now introduce the shell formulation used which is based on a degenerated 3D variational formulation by imposing two basic assumptions. The first assumption is the *Reissner–Mindlin* kinematical assumption according to which a material straight line that is orthogonal to the mid-surface remains straight and unstretched during the deformations. The resulting displacement is

$$\mathbf{U}(\xi^1, \xi^2, \xi^3) = \mathbf{u}(\xi^1, \xi^2) + \xi^3 \boldsymbol{\theta}(\xi^1, \xi^2) \tag{10}$$

where $\mathbf{u}(\xi^1, \xi^2)$ is the displacement of the shell mid-surface and

$$\boldsymbol{\theta}(\xi^1, \xi^2) = \theta_\lambda(\xi^1, \xi^2) \mathbf{a}^\lambda(\xi^1, \xi^2) \tag{11}$$

is the surface rotation tensor giving the rotation of the straight line. Here $\mathbf{a}^\lambda(\xi^1, \xi^2)$ are the 2D contravariant base vectors and θ_λ are the covariant components of $\boldsymbol{\theta}$. Note that the displacements $\xi^3 \boldsymbol{\theta}(\xi^1, \xi^2)$ are due to the rotation of the straight line. The second assumption is the plane stress assumption expressed by $\sigma^{33} = 0$. Imposing both assumptions and using the kinematical assumption also in the test function

$$\mathbf{V}(\xi^1, \xi^2, \xi^3) = \mathbf{v}(\xi^1, \xi^2) + \xi^3 \boldsymbol{\eta}(\xi^1, \xi^2) \tag{12}$$

the modified 3D variational problem is

Find $\mathbf{U} \in \mathscr{V}$ such that

$$A(\mathbf{U}, \mathbf{V}) = F(\mathbf{V}) \quad \forall\, \mathbf{V} \in \mathscr{V} \tag{13}$$

where the trial and test space $\mathscr{V}$ consists of usual Sobolev spaces of functions from $H^1(\Omega)$ whose traces vanish on Γ_D

$$\mathscr{V} = \{(\mathbf{v}, \boldsymbol{\eta}) \in [H^1(\Omega)]^3 \times [H^1(\Omega)]^2 \colon \mathbf{v} = \mathbf{0}, \boldsymbol{\eta} = \mathbf{0} \text{ on } \Gamma_D\} \tag{14}$$

The bilinear form $A(\mathbf{U}, \mathbf{V})$ and the linear form $F(\mathbf{V})$ are given by

$$A(\mathbf{U}, \mathbf{V}) = \int_\Omega [C^{\alpha\beta\lambda\mu} e_{\alpha\beta}(\mathbf{U}) e_{\lambda\mu}(\mathbf{V}) + D^{\alpha\lambda} e_{\alpha 3}(\mathbf{U}) e_{\lambda 3}(\mathbf{V})] \, \mathrm{d}V \tag{15}$$

$$F(\mathbf{V}) = \int_\Omega \mathbf{F} \cdot \mathbf{V} \, \mathrm{d}V \tag{16}$$

with $\mathrm{d}V = \sqrt{g} \, \mathrm{d}\xi^1 \, \mathrm{d}\xi^2 \, \mathrm{d}\xi^3$ and

$$C^{\alpha\beta\lambda\mu} = \frac{E}{2(1+\nu)} \left(g^{\alpha\lambda} g^{\beta\mu} + g^{\alpha\mu} g^{\beta\lambda} + \frac{2\nu}{1-\nu} g^{\alpha\beta} g^{\lambda\mu} \right) \tag{17}$$

$$D^{\alpha\lambda} = \frac{2E}{1+\nu} g^{\alpha\lambda} \tag{18}$$

Hence, the contravariant stress components are

$$\sigma^{\alpha\beta} = C^{\alpha\beta\lambda\mu} e_{\lambda\mu} \tag{19}$$

$$\sigma^{\alpha 3} = \tfrac{1}{2} D^{\alpha\lambda} e_{\lambda 3} \tag{20}$$

The variational formulation (13) represents a mathematical shell model—referred to as the 'basic shell model' in References [3, 12]—since the unknowns are given by sets of tensors defined only on the shell mid-surface. Note that the e_{33} component of the strain tensor does not appear in the bilinear form defined in (15) because of the plane stress assumption $\sigma^{33} = 0$ (which is also imposed to obtain (19)).

2.2. *Finite element discretization*

The shell finite element discretization to be used is based on the degenerated 3D variational formulation given in References [3, 10]. For the approximation of the shell geometry, the general isoparametric concept is employed such that the position vector $\mathbf{x}_h(r, s, z)$ inside an element is described by the equation

$$\mathbf{x}_h(r, s, z) = \sum_{i=1}^{n} h_i(r, s) \mathbf{x}^{(i)} + \frac{z}{2} \sum_{i=1}^{n} t^{(i)} h_i(r, s) \mathbf{a}_3^{(i)} \tag{21}$$

where the $h_i(r, s)$ are the usual 2D shape functions associated with the n nodes of the element considered, $\mathbf{x}^{(i)}$ are the co-ordinates of node (i), and (r, s, z) are the local isoparametric element co-ordinates. The quantities $t^{(i)}$ and $\mathbf{a}_3^{(i)}$ denote the thickness and the unit normal vector at node (i), respectively. Hence, with this strategy a 3D discretization of the shell structure is obtained by simply using standard 2D shape functions.

Using the isoparametric concept, the displacement and rotation fields are interpolated with the same shape functions as used in the approximation of the geometry. Hence, for the

finite element solution $\mathbf{U}_h(r,s,z)$ and for the test functions $\mathbf{V}_h(r,s,z)$ we use

$$\mathbf{U}_h(r,s,z) = \sum_{i=1}^{n} h_i(r,s)\mathbf{u}_h^{(i)} + \frac{z}{2}\sum_{i=1}^{n} t^{(i)}h_i(r,s)\boldsymbol{\theta}_h^{(i)} \tag{22}$$

$$\mathbf{V}_h(r,s,z) = \sum_{i=1}^{n} h_i(r,s)\mathbf{v}_h^{(i)} + \frac{z}{2}\sum_{i=1}^{n} t^{(i)}h_i(r,s)\boldsymbol{\eta}_h^{(i)} \tag{23}$$

where $\mathbf{u}_h^{(i)}$ and $\mathbf{v}_h^{(i)}$ denote the displacements and $\boldsymbol{\theta}_h^{(i)}$ and $\boldsymbol{\eta}_h^{(i)}$ the rotations at the nodes. Introducing the finite element subspace $\mathscr{V}_h \subset \mathscr{V}$, the discrete variational problem can be written as

Find $\mathbf{U}_h \in \mathscr{V}_h$ such that

$$A_h(\mathbf{U}_h, \mathbf{V}_h) = F_h(\mathbf{V}_h) \quad \forall\, \mathbf{V}_h \in \mathscr{V}_h \tag{24}$$

where the subscript h in $A_h(.,.)$ and $F_h(.)$ indicates that we are using the approximated geometry defined by (21) to compute the bilinear and linear forms. We denote with $\boldsymbol{\Omega}_h$ the 3D approximate geometry, which in general is different from the actual reference domain $\boldsymbol{\Omega}$. Note that we use the local co-ordinate system (r,s,z) within each element instead of (ξ^1, ξ^2, ξ^3) [3].

The variational problem given in (24) corresponds to a pure displacement-based finite element shell model. As is well known, this formulation leads to large errors in the finite element solution as the thickness tends to zero (the finite element discretization 'locks'). The solution errors are particularly large when using low-order interpolations. To circumvent this problem, an effective approach is to employ MITC shell elements.

2.3. MITC shell finite elements

The underlying idea of MITC shell elements is to interpolate the strains within each element using a specific interpolation strategy, instead of using the strain components directly computed from the displacements [10, 13, 14]. In order to carry out the MITC interpolation, a set of the so-called tying points is defined for each strain component. Considering the covariant components of the strain tensor $e_{ij}(r,s,z)$ in the local co-ordinate system (r,s,z), the tying procedure corresponds to a reduction operator R_h acting on the 3D strains such that

$$\hat{e}_{ij}(r,s,z) = R_h e_{ij}(r,s,z) \tag{25}$$

where $\hat{e}_{ij}(r,s,z)$ denotes the strain tensor obtained with the MITC tying procedure. The MITC discrete variational problem can be written as

Find a function $\hat{\mathbf{U}}_h \in \mathscr{V}_h$ such that

$$\hat{A}_h(\hat{\mathbf{U}}_h, \mathbf{V}_h) = F_h(\mathbf{V}_h) \quad \forall\, \mathbf{V}_h \in \mathscr{V}_h \tag{26}$$

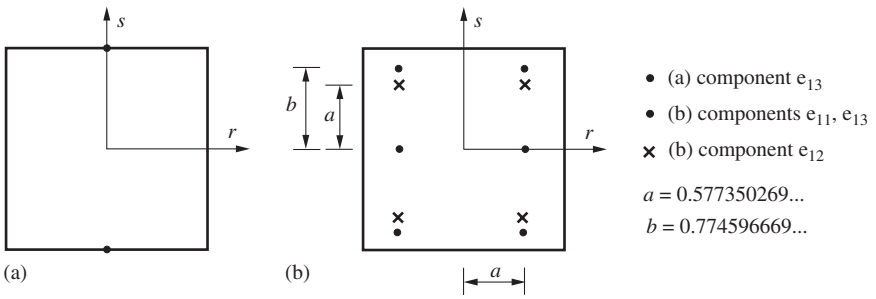

Figure 1. Tying points for the MITC shell elements: (a) MITC4 element; and (b) MITC9 element.

with the bilinear form

$$\hat{A}_h(\hat{\mathbf{U}}_h, \mathbf{V}_h) = \int_{\Omega_h} [C^{\alpha\beta\lambda\mu}\hat{e}_{\alpha\beta}(\hat{\mathbf{U}}_h)\hat{e}_{\lambda\mu}(\mathbf{V}_h) + D^{\alpha\lambda}\hat{e}_{\alpha 3}(\hat{\mathbf{U}}_h)\hat{e}_{\lambda 3}(\mathbf{V}_h)]\,\mathrm{d}V \tag{27}$$

where the '$\hat{}$' symbol indicates that we are using the MITC rule in (25) to interpolate the strains in the calculation of the bilinear form. We also distinguish between $\mathbf{U}_h$, which is the finite element solution of the displacement-based shell model, and $\hat{\mathbf{U}}_h$, which is the solution of the MITC finite element shell model. Of course, the bilinear form in (26) depends on the specific MITC element used and must satisfy the convergence requirements [3, 11].

In this paper, we only consider the quadrilateral MITC4 and MITC9 elements [14–16]. The MITC4 element is formulated using four nodal points having five degrees of freedom each (three displacements and two rotations on the shell mid-surface), while the MITC9 element is based on nine nodal points. Note that in the MITC4 formulation only the transverse shears $e_{\alpha 3}$ are subject to the tying procedure, while for the MITC9 shell element every component of the strain tensor is calculated with the MITC rule (see Figure 1). The MITC procedure can also be related to a mixed formulation using the Hellinger–Reissner functional [10, 13, 14].

Since the evaluation of influence functions for stress quantities is based on the calculation of the stresses corresponding to the element formulation, we may note the following: After calculating the covariant strains using the MITC procedure based on (25), the contravariant stress components can be calculated either by using (19) and (20) with the strains $\hat{e}_{ij}$ instead of e_{ij}, or by first calculating the strain tensor components $\hat{\mathbf{e}}_{\text{glob}}$ corresponding to the global Cartesian co-ordinate system using

$$\hat{\mathbf{e}}_{\text{glob}} = \sum_{i=1}^{3}\sum_{j=1}^{3} \hat{e}_{ij}(\mathbf{g}^i \otimes \mathbf{g}^j) \tag{28}$$

The corresponding stresses can then be calculated by applying a 3D formulation of Hooke's stress strain law with respect to the global Cartesian co-ordinate system that takes into account the assumption $\sigma^{33} = 0$. Of course, these global stresses can easily be transformed back to a local Cartesian co-ordinate system $(\bar{r}, \bar{s}, \bar{z})$ [10].

Table I. Examples for the thickness parameter $\varepsilon = t/L$.

	t	L	$\varepsilon = t/L$
Egg	0.3 mm	60 mm	5×10^{-3}
Earth's crust	50 km	12 650 km	4×10^{-3}
Cooling tower	0.2 m	100 m	2×10^{-3}
Sheet of paper	0.1 mm	200 mm	5×10^{-4}
Engine hood	0.75 mm	1500 mm	5×10^{-4}

3. ASYMPTOTIC BEHAVIOUR OF SHELLS

Shell structures are 3D structures with one dimension, the thickness, small compared to the other two dimensions. As a consequence, a shell structure will carry its load by bending action, by membrane action and, many times in practice, by combined bending and membrane actions. To precisely categorize shell behaviour we study the asymptotic behaviour of the structure as the thickness decreases [2, 3]. For this purpose we introduce a dimensionless thickness parameter ε defined by

$$\varepsilon = \frac{t}{L} \tag{29}$$

where L denotes an overall characteristic length of the shell and t is the thickness (some examples for the thickness parameter ε are given in Table I). Using this thickness parameter, the shell variational problem (13) can be studied by focusing on the problem

$$\varepsilon^3 A_\mathrm{b}(\mathbf{U}, \mathbf{V}) + \varepsilon A_\mathrm{m}(\mathbf{U}, \mathbf{V}) = G(\mathbf{V}) \quad \forall\, \mathbf{V} \in \mathscr{V} \tag{30}$$

where $A_\mathrm{b}(.\,,.)$ and $A_\mathrm{m}(.\,,.)$ capture, respectively, the bending and membrane/shear energy and $G(.)$ is a scaled linear form.

As discussed in References [2, 3], the subspace $\mathscr{V}_0$ takes on a crucial role

$$\mathscr{V}_0 = \{\mathbf{V} \in \mathscr{V} \mid A_\mathrm{m}(\mathbf{V}, \mathbf{V}) = 0\} \tag{31}$$

The subspace $\mathscr{V}_0$ contains all those displacements for which the membrane/shear energy is zero, hence it is also called the subspace of pure bending displacements. Clearly, $\mathscr{V}_0$ may be trivial, i.e. $\mathscr{V}_0 = \{\mathbf{0}\}$. This situation is referred to as 'inhibited pure bending'. The asymptotic behaviour of shell structures is highly dependent on whether pure bending is inhibited or not. In the situation of 'inhibited pure bending', the load may or may not correspond to an 'admissible' membrane loading. This is expressed as $G(\mathbf{V}) \in \mathscr{V}_\mathrm{m}'$ or $G(\mathbf{V}) \notin \mathscr{V}_\mathrm{m}'$ where $\mathscr{V}_\mathrm{m}$ is the space of displacements having bounded membrane and shear energy only. The asymptotic behaviour will then correspond, respectively, to a pure membrane-dominated or a mixed shell problem. On the other hand, in the situation of 'non-inhibited pure bending' that is when $\mathscr{V}_0 \neq \{\mathbf{0}\}$, we frequently observe the bending-dominated state, where the membrane/shear energy term $A_\mathrm{m}(\mathbf{V}, \mathbf{V})$ asymptotically vanishes. However, this limit case holds only when the load activates the pure bending displacements, otherwise the theoretical asymptotic behaviour is membrane-dominated or mixed, but in each case unstable (see Table II).

Table II. Classification of shell asymptotic behaviours.

Case	Loading	Category
Non-inhibited shell $\mathscr{V}_0 \neq \{\mathbf{0}\}$	Loading activates pure-bending $\exists \mathbf{V} \in \mathscr{V}_0$ such that $G(\mathbf{V}) \neq 0$	(i) Bending-dominated
	Loading does not activate pure-bending $G(\mathbf{V}) = 0 \ \forall \mathbf{V} \in \mathscr{V}_0$	(ii) Membrane-dominated or mixed, but unstable
Inhibited shell $\mathscr{V}_0 = \{\mathbf{0}\}$	Admissible membrane loading $G \in \mathscr{V}'_{\mathrm{m}}$	(iii) Membrane-dominated
	Non-admissible membrane loading $G \neq \mathscr{V}'_{\mathrm{m}}$	(iv) Mixed shell problem

Influence functions, by their very nature, are independent of the actual loading. Hence, it is valuable to study both cases of shells, namely shells for which $\mathscr{V}_0 = \{\mathbf{0}\}$ and $\mathscr{V}_0 \neq \{\mathbf{0}\}$. The influence function should reveal the basic load carrying characteristics of the structures.

It is important to mention that the shell model based on the variational formulation (13) exhibits the same asymptotic behaviour as classical shell models, for example of Koiter type. Hence, when the thickness parameter ε approaches zero, the solution of the basic 3D mathematical shell model converges to the same limit solution as the classical shell models.

4. CALCULATION OF INFLUENCE FUNCTIONS

In the engineering design process, influence functions are typically used to study the behaviour (and to find the maximum value) of a specific quantity of interest while the load is moving. Typical fields of application are the analysis of bridges or cranes in structural engineering, although influence functions may also be useful in the automotive or aircraft industry, where many load cases have to be considered.

4.1. General approach

Historically, influence functions are solely calculated for point quantities such as displacements or internal forces of beams and trusses. However, motivated by the recent goal-oriented error estimation procedures, this view is broadened by considering generalized influence functions for quantities of interest, which can be *any* individual (but linear) quantity that has a proper meaning in the solution space. For instance, the quantity of interest, denoted by $Q(\mathbf{U})$, can be the mean value of a specific stress component integrated over a patch Ω_ρ of the domain Ω

$$Q(\mathbf{U}) = |\Omega_\rho|^{-1} \int_{\Omega_\rho} \sigma_{ij}(\mathbf{U}) \, \mathrm{d}V \tag{32}$$

where the patch can be chosen small. Another example is the traction over a portion Γ_ρ of the boundary Γ_{D} of the domain so that the quantity of interest is

$$Q(\mathbf{U}) = \int_{\Gamma_\rho} \sigma_{ij}(\mathbf{U}) n_j \, \mathrm{d}\Gamma \tag{33}$$

Of course, we are also free in the choice of the co-ordinate system for the definition of the quantity of interest, so that $Q(\mathbf{U})$ can be defined in any chosen co-ordinate system.

From a mathematical point of view, it is convenient to regard the quantity of interest as a bounded, linear functional $Q: \mathscr{V} \to \mathbb{R}$ in the dual space $\mathscr{V}'$ associated with the norm

$$\|Q\|_{\mathscr{V}'} = \sup_{\mathbf{V} \in \mathscr{V}} \frac{Q(\mathbf{V})}{\|\mathbf{V}\|_{\mathscr{V}}} \tag{34}$$

Considering the problem in (13), since $\mathscr{V}$ is a Hilbert space associated with the bilinear form $A(.,.)$ we can employ the Riesz representation theorem which asserts that there is a unique solution of the variational problem:

Find $\mathbf{Z} \in \mathscr{V}$ such that

$$A(\mathbf{Z}, \mathbf{V}) = Q(\mathbf{V}) \quad \forall \mathbf{V} \in \mathscr{V} \tag{35}$$

The solution of this problem is referred to as the dual solution and can be interpreted as the generalized influence function related to the functional (or quantity of interest) $Q(\mathbf{V})$.

Of course, the influence function is generally unknown so that a finite element method has to be employed. The finite element approximation of the influence function $\mathbf{Z} \in \mathscr{V}$ is obtained by solving the discrete problem:

Find $\mathbf{Z}_h \in \mathscr{V}_h$ such that

$$A_h(\mathbf{Z}_h, \mathbf{V}_h) = Q_h(\mathbf{V}_h) \quad \forall \mathbf{V}_h \in \mathscr{V}_h \tag{36}$$

Clearly, for the computation of the bilinear form as well as for the computation of the functional of interest we use the same finite element discretization as we use for the primal finite element analysis to obtain $\mathbf{U}_h$.

4.2. Influence functions for MITC discretizations

Although the procedure to calculate the influence function is general, we detail our strategy for the MITC approach of discretization. Then according to (26) and (35), the discrete problem to solve for the influence function using the MITC procedure is

Find the function $\hat{\mathbf{Z}}_h \in \mathscr{V}_h$ such that

$$\hat{A}_h(\hat{\mathbf{Z}}_h, \mathbf{V}_h) = \hat{Q}_h(\mathbf{V}_h) \quad \forall \mathbf{V}_h \in \mathscr{V}_h \tag{37}$$

where $\hat{\mathbf{Z}}_h \in \mathscr{V}_h$ denotes the influence function obtained with the MITC procedure. Assuming that the same finite element space $\mathscr{V}_h$ is employed in the solution of the primal problem, see (26), as in the solution of the influence function, see (37), it follows from (16), (26), and (37) that the influence function satisfies the following 'consistency condition':

$$\hat{Q}_h(\hat{\mathbf{U}}_h) = \hat{A}_h(\hat{\mathbf{Z}}_h, \hat{\mathbf{U}}_h) = \hat{A}_h(\hat{\mathbf{U}}_h, \hat{\mathbf{Z}}_h) = \int_{\Omega_h} \mathbf{F} \cdot \hat{\mathbf{Z}}_h \, \mathrm{d}V \tag{38}$$

Hence—as is usual when influence functions are employed in structural engineering—the integration of the load $\mathbf{F}$ multiplied by the influence function $\hat{\mathbf{Z}}_h$ yields the same quantity of interest $\hat{Q}_h(\hat{\mathbf{U}}_h)$ as the primary finite element analysis based on (26). In this primary finite

element analysis we would solve (26) and then simply evaluate the quantity of interest, i.e. for the example in (32),

$$\hat{Q}_h(\hat{\mathbf{U}}_h) = |\Omega_{h,\rho}|^{-1} \int_{\Omega_{h,\rho}} \hat{\sigma}_{kl}(\hat{\mathbf{U}}_h)\,\mathrm{d}V \tag{39}$$

where $\Omega_{h,\rho}$ is the considered patch in the finite element discretization. Hence, there are always these two equivalent approaches to evaluate a quantity of interest.

In order to calculate the load vector corresponding to the right-hand side of (37), we employ the definition of the quantity of interest. For example, if the quantity of interest is as in (39), we have to evaluate for certain interpolation functions $h_i(r,s) \in \mathscr{V}_h$ the expression

$$\hat{Q}_h^{(i)}(h_i(r,s)) = |\Omega_{h,\rho}|^{-1} \int_{\Omega_{h,\rho}} \hat{\sigma}_{kl}(h_i(r,s))\,\mathrm{d}V \tag{40}$$

In other words: for every 'unit displacement field' $h_i(r,s) \in \mathscr{V}_h$ (which also contains the unit rotation fields, see (22)) we have to calculate the corresponding mean value of the MITC-stresses $\hat{\sigma}_{kl}$. Clearly, expression (40) can be evaluated on the element level for every interpolation function $h_i(r,s)$ and assembled afterwards. For instance, using MITC4 shell finite elements, expression (40) has to be evaluated 20 times for every element. Of course, expression (40) has to be evaluated only for the elements in $\Omega_{h,\rho}$, i.e. only for those elements for which the quantity $\hat{Q}_h^{(i)}$ is not known *a priori* to be zero.

4.3. Influence functions for specific quantities of interest

In some shell analyses, we require shear forces and bending moments. In the case of bending moments we may define the quantity of interest as

$$Q(\mathbf{U}) = M_{\bar{r}} = \int_{\Omega_\rho} \bar{z}\,\sigma_{\bar{r}\bar{r}}(\mathbf{U})\,\mathrm{d}V \tag{41}$$

where $\sigma_{\bar{r}\bar{r}}$ are the axial stresses in the $\bar{r}$ direction in a local Cartesian co-ordinate system and $\bar{z}$ denotes the corresponding moment arm. Hence, $Q(\mathbf{U})$ can then be interpreted as an integrated bending moment on the patch Ω_ρ. In this case, the equivalent nodal forces to calculate the influence function correspond to the element bending moments which are a result of the unit displacement fields.

It might also be useful to study the influence function for point values. However, point values of the solution are not well defined in $H^1(\Omega)$ in two or three dimensions. Hence, some regularization is necessary where we consider a local average of the quantity of interest such as

$$Q(\mathbf{U}) = |\mathscr{B}_{\bar{\varepsilon}}|^{-1} \int_{\mathscr{B}_{\bar{\varepsilon}}} \sigma_{ij}(\mathbf{U})\,\mathrm{d}V = \sigma_{ij}(\mathbf{U})|_{\mathbf{x}_p} + O(\bar{\varepsilon}^2) \tag{42}$$

in which the radius $\bar{\varepsilon}$ of a ball $\mathscr{B}_{\bar{\varepsilon}} \subset \Omega$ around the point of interest $\mathbf{x}_p$ can be chosen small.

5. GOAL-ORIENTED ERROR ESTIMATION

A posteriori error estimation procedures have become an important tool for assessing the reliability and accuracy of finite element computations [7, 17]. These techniques have been

extended to the so-called goal-oriented error estimations where the error is estimated in some output data of engineering interest [7–9, 18–24]. The essential tool for estimating the error in such a quantity of interest is the influence function which filters out the necessary information for an accurate error estimate. Hence, the procedures derived in Section 4 to calculate influence functions can be directly applied.

Goal-oriented error estimation procedures have been successfully applied to linear and non-linear problems of solid mechanics as well as to problems of fluid mechanics and transient analyses. There are still open questions regarding the application to multi-physics problems (like fluid flow structural interactions) and, also, the use in shell structural analysis needs still to be developed when using a genuine shell formulation as we propose here. In the following, we present an efficient goal-oriented error estimation technique that takes into account the geometry error as well as the cancellation effect of the error over the analysis domain to address the issue of over-estimation.

5.1. Considerations regarding the approximation of the geometry

The finite element discretization of shell structures comprises generally two kinds of errors, namely, due to the interpolation of the displacements and the geometry. The geometry error is much more relevant in shell structural analysis than in the analyses of 2D or 3D solids. In the analysis of solids the approximation of the geometry affects only the boundary of the domain while in shell analysis the geometry error pertains to the whole domain. Hence, the influence of the actual geometry in the error estimation can be significant. In particular, the use of flux projection error estimators may be problematic, since they are only based on the analysis of discontinuities in the finite element solution and do not use any information on the actual geometry [25].

In the following we separate the error in the geometry approximation from the displacement interpolation error. For this purpose, we consider the variational problem:

Find $\mathbf{U}^* \in \mathscr{V}^*$ such that

$$A_h(\mathbf{U}^*, \mathbf{V}) = F_h(\mathbf{V}) \quad \forall\, \mathbf{V} \in \mathscr{V}^* \tag{43}$$

where $\mathscr{V}^* = \mathscr{V}^*(\Omega_h)$ denotes the continuous functional space defined on the finite element domain Ω_h. The corresponding finite element problem is

Find $\mathbf{U}_h \in \mathscr{V}_h \subset \mathscr{V}^*$ such that

$$A_h(\mathbf{U}_h, \mathbf{V}_h) = F_h(\mathbf{V}_h) \quad \forall\, \mathbf{V}_h \in \mathscr{V}_h \subset \mathscr{V}^* \tag{44}$$

The variational problem in (43) denotes an auxiliary problem of which $\mathbf{U}^*$ is the exact solution obtained on the finite element domain Ω_h and hence the subscript h refers to the geometry given by Ω_h only. Then the error between the exact solution and the finite element solution can be written as

$$\begin{aligned} \mathbf{E} &= \mathbf{U} - \mathbf{U}_h \\ &= (\mathbf{U} - \mathbf{U}^*) + (\mathbf{U}^* - \mathbf{U}_h) = \mathbf{E}^* + \mathbf{E}_h^* \end{aligned} \tag{45}$$

In the same manner, let $Q(\mathbf{U})$ denote the (exact) quantity of interest and $Q_h(\mathbf{U}_h)$ its finite element approximation, then the error quantity, for which we seek an estimate, can be decomposed as follows:

$$Q(\mathbf{E}) = Q(\mathbf{U}) - Q_h(\mathbf{U}_h) \tag{46}$$

$$= \underbrace{(Q(\mathbf{U}) - Q_h(\mathbf{U}^*))}_{\text{geometry error}} + \underbrace{(Q_h(\mathbf{U}^*) - Q_h(\mathbf{U}_h))}_{\text{displacement interpolation error}} \tag{47}$$

In general it is not feasible to exactly evaluate the geometry and displacement interpolation errors. Hence, in the following we design some error estimates, which can be classified into error estimates for the displacement interpolation error only, and into error estimates that take also into account the error in the geometry approximation. The reason we focus on error estimates for the displacement interpolation error only is to provide a natural extension of well-known goal-oriented error estimates for the use in shell finite element analysis.

5.2. Error estimates for the displacement interpolation error

When designing estimates for the displacement interpolation error only, we tacitly assume that the geometry error is negligible, which holds true if the geometry is simple or a sufficiently large number of elements is used to approximate the geometry.[‡] Then the error in the quantity of interest reduces to

$$Q_h(\mathbf{E}_h^*) = Q_h(\mathbf{U}^*) - Q_h(\mathbf{U}_h) \tag{48}$$

The dual problem to the variational problem in (43) is

Find $\mathbf{Z}^* \in \mathscr{V}^*$ such that

$$A_h(\mathbf{Z}^*, \mathbf{V}) = Q_h(\mathbf{V}) \quad \forall\, \mathbf{V} \in \mathscr{V}^* \tag{49}$$

Provided that $\mathscr{V}_h \subset \mathscr{V}^*$ we may consider (49) using $\mathbf{V}_h$

$$A_h(\mathbf{Z}^*, \mathbf{V}_h) = Q_h(\mathbf{V}_h) \quad \forall\, \mathbf{V}_h \in \mathscr{V}_h \subset \mathscr{V}^* \tag{50}$$

Then choosing $\mathbf{V} = \mathbf{U}^*$ in (49) and $\mathbf{V}_h = \mathbf{U}_h$ in (50) yields the error representation

$$Q_h(\mathbf{E}_h^*) = A_h(\mathbf{Z}^*, \mathbf{U}^* - \mathbf{U}_h) \tag{51}$$

Employing the fundamental Galerkin orthogonality with $\mathbf{V}_h \in \mathscr{V}_h$, we obtain the starting point of our error estimate

$$Q_h(\mathbf{E}_h^*) = A_h(\mathbf{Z}^* - \mathbf{V}_h, \mathbf{U}^* - \mathbf{U}_h) \tag{52}$$

[‡]*A priori* error estimates for the total error of shell finite element discretizations are given in Reference [3], where it is shown that the error of a continuum mechanics displacement-based shell model measured in the $\mathscr{V}$-norm is usually of the order $O(h^{\min\{p,2\}})$ with p denoting the order of the interpolation functions, but optimal convergence (when $p > 2$) can also be recovered [3, 26].

There are several strategies available to estimate the magnitude of $Q_h(\mathbf{E}_h^*)$. One strategy is to apply the Cauchy–Schwarz inequality to (52) and choose $\mathbf{V}_h = \mathbf{Z}_h$ which yields the upper bound

$$|Q_h(\mathbf{E}_h^*)| \leqslant \|\mathbf{Z}^* - \mathbf{Z}_h\|_E \|\mathbf{U}^* - \mathbf{U}_h\|_E \tag{53}$$

However, error bounds as in (53) are expected to heavily over-estimate the true error due to the lack of the cancellation effect of errors over the analysis domain as discussed in Reference [27]. On the other hand, applying the Cauchy–Schwarz inequality elementwise to (52) may lead to useful error indicators for driving mesh adaptivity, although over-refinement due to over-estimation is still an issue.

A more effective way to obtain error bounds on the quantity of interest is to employ the techniques in the dual-weighted residual (DWR) method as proposed by Bangerth and Rannacher [7], Becker and Rannacher [8] and Rannacher and Suttmeier [9]. Here, we reorganize (52) as follows:

$$Q_h(\mathbf{E}_h^*) = A_h(\mathbf{Z}^* - \mathbf{V}_h, \mathbf{U}^* - \mathbf{U}_h) \tag{54}$$

$$= F_h(\mathbf{Z}^* - \mathbf{V}_h) - A_h(\mathbf{U}_h, \mathbf{Z}^* - \mathbf{V}_h) \tag{55}$$

and apply integration by parts elementwise to the remaining bilinear form so that with $\bigcup \Omega_k = \Omega_h$ the error representation becomes

$$Q_h(\mathbf{E}_h^*) = \sum_{\Omega_k} \left\{ \int_{\Omega_k} \mathbf{R}_h \cdot (\mathbf{Z}^* - \mathbf{V}_h)\, \mathrm{d}V + \int_{\Gamma_k} \mathbf{J}_h \cdot (\mathbf{Z}^* - \mathbf{V}_h)\, \mathrm{d}\Gamma \right\} \tag{56}$$

where $\mathbf{R}_h$ denotes the element residuals of the primal problem

$$\mathbf{R}_h = \operatorname{div} \boldsymbol{\sigma}_h + \mathbf{F} \quad \text{on } \Omega_k \tag{57}$$

Here $\boldsymbol{\sigma}_h = [\sigma_h^{ij}]$ is the finite element stress tensor and $\mathbf{J}_h$ represents the jumps of the tractions at the element edges Γ_k computed by contributions of the element Ω_k and the adjacent element Ω_k'

$$\mathbf{J}_h = \begin{cases} \frac{1}{2}(\boldsymbol{\sigma}_h \mathbf{n}_h + \boldsymbol{\sigma}_h' \mathbf{n}_h') & \text{at } \Gamma_k \not\subseteq \Gamma \\ \boldsymbol{\sigma}\mathbf{n}_h - \boldsymbol{\sigma}_h \mathbf{n}_h & \text{at } \Gamma_{\mathrm{N}} \\ \mathbf{0} & \text{at } \Gamma_{\mathrm{D}} \end{cases} \tag{58}$$

with $\mathbf{n}_h$ denoting the unit outward normal vector to Γ_k. To steer an adaptive mesh refinement process, the following element error indicators can be used:

$$\eta_k = |(\mathbf{R}_h, \mathbf{Z}^* - \mathbf{V}_h)_{\Omega_k} + (\mathbf{J}_h, \mathbf{Z}^* - \mathbf{V}_h)_{\Gamma_k}| \tag{59}$$

which yield the guaranteed upper error bound

$$|Q_h(\mathbf{E}_h^*)| \leqslant \sum_{\Omega_k} \eta_k \tag{60}$$

There are several approaches for evaluating the unknown dual solution $\mathbf{Z}^*$ and for choosing the test function $\mathbf{V}_h$ used in (56). As proposed in Reference [7], and also discussed in

Reference [28], one possibility is to obtain an approximation of $\mathbf{Z}^*$ using a higher-order method where, for instance, biquadratic functions are used instead of bilinear functions, and choosing for $\mathbf{V}_h$ an interpolant. Another technique approximates the exact dual solution by employing higher-order interpolation functions defined over single patches of the domain.

In order to extend goal-oriented error estimates for use with MITC shell elements, we consider

$$\hat{Q}_h(\hat{\mathbf{E}}_h^*) = \hat{Q}_h(\mathbf{U}^*) - \hat{Q}_h(\hat{\mathbf{U}}_h) \tag{61}$$

$$\approx \hat{A}_h(\mathbf{Z}^* - \hat{\mathbf{Z}}_h, \mathbf{U}^* - \hat{\mathbf{U}}_h) \tag{62}$$

where (61) denotes the error in the quantity of interest between the exact solution and the MITC solution, both obtained on the finite element domain Ω_h.

For the mixed formulation, we employ the s-norm proposed in Reference [11], which compares the approximate and exact strains by means of the governing energy, hence representing a norm equivalent to the classical energy norm of a displacement-based shell model. Regarding the error in the primal and the dual solution the s-norm is, respectively, defined by

$$\begin{aligned}\|\mathbf{U}^* - \hat{\mathbf{U}}_h\|_s^2 = \int_{\Omega_h} [&C^{\alpha\beta\lambda\mu}(e_{\alpha\beta}(\mathbf{U}^*) - \hat{e}_{\alpha\beta}(\hat{\mathbf{U}}_h))(e_{\lambda\mu}(\mathbf{U}^*) - \hat{e}_{\lambda\mu}(\hat{\mathbf{U}}_h)) \\ &+ D^{\alpha\lambda}(e_{\alpha 3}(\mathbf{U}^*) - \hat{e}_{\alpha 3}(\hat{\mathbf{U}}_h))(e_{\lambda 3}(\mathbf{U}^*) - \hat{e}_{\lambda 3}(\hat{\mathbf{U}}_h))]\,\mathrm{d}V\end{aligned} \tag{63}$$

$$\begin{aligned}\|\mathbf{Z}^* - \hat{\mathbf{Z}}_h\|_s^2 = \int_{\Omega_h} [&C^{\alpha\beta\lambda\mu}(e_{\alpha\beta}(\mathbf{Z}^*) - \hat{e}_{\alpha\beta}(\hat{\mathbf{Z}}_h))(e_{\lambda\mu}(\mathbf{Z}^*) - \hat{e}_{\lambda\mu}(\hat{\mathbf{Z}}_h)) \\ &+ D^{\alpha\lambda}(e_{\alpha 3}(\mathbf{Z}^*) - \hat{e}_{\alpha 3}(\hat{\mathbf{Z}}_h))(e_{\lambda 3}(\mathbf{Z}^*) - \hat{e}_{\lambda 3}(\hat{\mathbf{Z}}_h))]\,\mathrm{d}V\end{aligned} \tag{64}$$

Using these norms it should be possible to obtain an error bound like in (53), based on the error representations (61) and (62). However, we do not pursue this approach because the resulting error measure would not contain the error cancellation effect over the analysis domain mentioned above.

In the same manner it should be possible to obtain an approximate error representation equivalent to (56) in which the MITC solution would be used to calculate the residuals and jumps as defined in (57) and (58). We do not proceed this way either since we rather want to derive error measures that also take into account the error in the geometry approximation.

5.3. Error estimates on the displacement and geometry approximations

We next set out to design a goal-oriented error estimate that allows to assess efficiently and simultaneously the error in the geometry and displacement interpolations. Consider, theoretically the use of a reference solution obtained with a very fine reference mesh for the reference domain Ω_{ref} very close to Ω. Let $\mathbf{U}_{\mathrm{ref}}$ be the reference solution that is a very accurate approximation of $\mathbf{U}$ such that $\mathbf{U}_{\mathrm{ref}} \in \mathscr{V}_{\mathrm{ref}} \subset \mathscr{V}$ with $\mathscr{V}_{\mathrm{ref}} = \mathscr{V}_{\mathrm{ref}}(\Omega_{\mathrm{ref}})$. Then the reference error $\mathbf{E}_h = \mathbf{U}_{\mathrm{ref}} - \mathbf{U}_h$ is a good approximation to the exact error $\mathbf{E}$. Thus, in the error estimate for the quantity of interest we consider

$$Q_{\mathrm{ref}}(\mathbf{E}_h) = Q_{\mathrm{ref}}(\mathbf{U}_{\mathrm{ref}}) - Q_h(\mathbf{U}_h) \tag{65}$$

In other words, we assume that the geometry error between the exact and reference fine mesh geometries is negligible, which is evident if a sufficiently large number of elements is used to obtain the reference solution. Of course, we do not want to calculate $Q_{\text{ref}}(\mathbf{E}_h)$ but only obtain an estimate. The dual problem corresponding to the reference fine mesh is

Find $\mathbf{Z}_{\text{ref}} \in \mathscr{V}_{\text{ref}}$ such that

$$A_{\text{ref}}(\mathbf{Z}_{\text{ref}}, \mathbf{V}) = Q_{\text{ref}}(\mathbf{V}) \quad \forall\, \mathbf{V} \in \mathscr{V}_{\text{ref}} \tag{66}$$

where $\mathbf{Z}_{\text{ref}} \in \mathscr{V}_{\text{ref}}$ denotes the reference solution of the dual problem on the fine reference mesh. A simple and direct approach to obtain error measures is then to consider

$$Q_{\text{ref}}(\mathbf{E}_h) = A_{\text{ref}}(\mathbf{Z}_{\text{ref}}, \mathbf{U}_{\text{ref}}) - A_h(\mathbf{Z}_h, \mathbf{U}_h) \tag{67}$$

$$= F_{\text{ref}}(\mathbf{Z}_{\text{ref}}) - F_h(\mathbf{Z}_h) \tag{68}$$

or

$$Q_{\text{ref}}(\mathbf{E}_h) = \int_{\Omega_{\text{ref}}} \mathbf{F} \cdot \mathbf{Z}_{\text{ref}}\, \mathrm{d}V - \int_{\Omega_h} \mathbf{F} \cdot \mathbf{Z}_h\, \mathrm{d}V \tag{69}$$

where in practical use, we need to replace the reference dual solution $\mathbf{Z}_{\text{ref}}$ by some approximation.

Clearly, the use of the error representation (69) can only be recommended if we wish to estimate the error in the quantity of interest for a given mesh without having the intention of mesh adaptivity; namely using (69), local information on the error may be cancelled. However, provided that $\mathscr{V}_h \subset \mathscr{V}_{\text{ref}}$ and $\bigcup \Omega_k = \Omega_h$ we can also obtain local error indicators for driving mesh adaptivity by considering

$$Q_{\text{ref}}(\mathbf{E}_h) \approx \sum_{\Omega_k} \left\{ \int_{\Omega_k} \mathbf{F} \cdot \mathbf{Z}_{\text{ref}}\, \mathrm{d}V - A_h(\mathbf{Z}_h, \mathbf{U}_h)_{\Omega_k} \right\} \tag{70}$$

In (70) the consistency error due to neglecting the overlap domain $\Omega_e = \Omega_{\text{ref}} \backslash \Omega_h$ in the first integral should be small and, at least, not essential for the use of (70) in mesh adaptivity.

Using the MITC4 element in a shell solution, we consider the error representation

$$\hat{Q}_{\text{ref}}(\hat{\mathbf{E}}_h) = \hat{Q}_{\text{ref}}(\hat{\mathbf{U}}_{\text{ref}}) - \hat{Q}_h(\hat{\mathbf{U}}_h) \tag{71}$$

$$= \hat{A}_{\text{ref}}(\hat{\mathbf{Z}}_{\text{ref}}, \hat{\mathbf{U}}_{\text{ref}}) - \hat{A}_h(\hat{\mathbf{Z}}_h, \hat{\mathbf{U}}_h) \tag{72}$$

$$= F_{\text{ref}}(\hat{\mathbf{Z}}_{\text{ref}}) - F_h(\hat{\mathbf{Z}}_h) \tag{73}$$

or, similar to (69) and (70),

$$\hat{Q}_{\text{ref}}(\hat{\mathbf{E}}_h) = \int_{\Omega_{\text{ref}}} \mathbf{F} \cdot \hat{\mathbf{Z}}_{\text{ref}}\, \mathrm{d}V - \int_{\Omega_h} \mathbf{F} \cdot \hat{\mathbf{Z}}_h\, \mathrm{d}V \tag{74}$$

$$\approx \sum_{\Omega_k} \left\{ \int_{\Omega_k} \mathbf{F} \cdot \hat{\mathbf{Z}}_{\text{ref}}\, \mathrm{d}V - \hat{A}_h(\hat{\mathbf{Z}}_h, \hat{\mathbf{U}}_h)_{\Omega_k} \right\} \tag{75}$$

We can now approximate the error representation in (74) by replacing the reference solution $\hat{\mathbf{Z}}_{\text{ref}}$ with an approximation obtained using a MITC9 shell element mesh

$$\hat{Q}_{\text{ref}}(\hat{\mathbf{E}}_h) \approx \int_{\Omega_{h9}} \mathbf{F} \cdot \hat{\mathbf{Z}}_h^{(\text{MITC9})} \, \mathrm{d}V - \int_{\Omega_h} \mathbf{F} \cdot \hat{\mathbf{Z}}_h \, \mathrm{d}V \tag{76}$$

where Ω_{h9} denotes the finite element reference domain using the MITC9 shell element mesh. In this equation, we use the same element size h for the MITC4 and MITC9 elements. Hence, the MITC9 element mesh consists of the same number of elements as used for obtaining $\hat{\mathbf{Z}}_h$, and we note that the additional nodes are located on the actual shell geometry. While we proceed in this way in all our example solutions, in principle of course also a finer MITC9 element mesh could be used, but then the cost of error estimation would increase.

In analogy to (75), for driving mesh adaptivity we might use

$$\hat{Q}_{\text{ref}}(\hat{\mathbf{E}}_h) \approx \sum_{\Omega_k} \left\{ \int_{\Omega_k} \mathbf{F} \cdot \hat{\mathbf{Z}}_h^{(\text{MITC9})} \, \mathrm{d}V - \hat{A}_h(\hat{\mathbf{Z}}_h, \hat{\mathbf{U}}_h)_{\Omega_k} \right\} \tag{77}$$

Clearly, the error representation in (76) is easy to evaluate and also takes into account the approximation of the geometry and the displacements. The relation also includes the cancellation effect of the error, so that the application to complex shell structures is promising. Of course, since the consistency condition (38) holds for both MITC4 and MITC9 approximations, the error estimate in (76) equals the difference in the quantity of interest between the MITC9 and MITC4 finite element solutions. On the other hand, once the influence function is available for both MITC9 and MITC4 discretizations, the error estimate is simple and the integrals in (76) can be evaluated for an arbitrary number of different load cases.

6. NUMERICAL EXAMPLES

In our numerical examples, goal-oriented error estimates are evaluated by using the approximate error representation (76). Hence, we always estimate the error for a given mesh discretized with MITC4 elements. In the error estimate we exclusively focus on the stresses defined in a local Cartesian co-ordinate system because of their physical relevance (rather than using stresses defined in a global Cartesian co-ordinate system). We only estimate the error for uniform meshes and do not employ any adaptivity. Indeed, since the error estimate uses the approximation of the exact influence function obtained with MITC9 elements, the calculation is carried out on the same mesh (with the same number of elements) by simply changing the element formulation to be used, which makes the procedure easy to implement. Of course, using the MITC9 element mesh, the shell geometry is represented more accurately since the additional nodes are on the actual shell geometry. For measuring the accuracy of our error estimate we use the effectivity index, which is the ratio between the estimated error using (76) and the calculated error using the reference solution defined in (73).

6.1. Cantilever beam cylindrical shell

In our first example, we calculate influence functions for the beam-like cylindrical shell problem shown in Figure 2(a), whose mechanical behaviour is similar to a cantilever beam. The finite

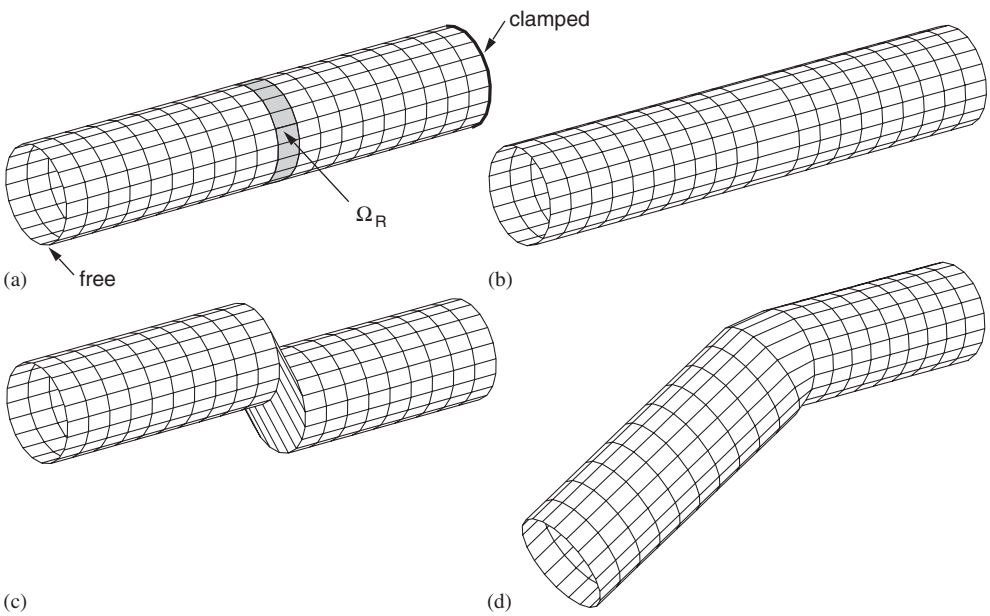

Figure 2. Influence functions for a cantilever beam cylindrical shell for different quantities of interest defined in the area Ω_R: (a) model description; (b) influence function for the integrated axial force; (c) influence function for the integrated shear force; and (d) influence function for the integrated bending moment.

element model consists of a 20×20 MITC4 shell element mesh and the thickness parameter is $\varepsilon = 10^{-3}$. The quantities of interest are, respectively, the integrated axial force, the integrated shear force, and the integrated bending moment in the radial domain Ω_R (see Figure 2(a)). Here, we expect influence functions similar to those of a cantilever beam, and exactly these are obtained for the axial force (Figure 2(b)) and the shear force (Figure 2(c)). Regarding the influence function for the integrated bending moment in Figure 2(d), the kink angle in classical beam theory is 45°. Here, we observe an error of 0.88% using the MITC4 element discretization while the error is zero when using the MITC9 element mesh.

6.2. Scordelis-Lo roof

The Scordelis-Lo roof as shown in Figure 3 is a membrane dominated shell problem provided that an admissible loading is used [2, 3, 29]. However, in the original version of this problem, the shell is subjected to self-weight loading which corresponds to a non-admissible membrane loading, so that the original Scordelis-Lo roof is a mixed shell problem. Note, that the diaphragms at the two ends refer to the boundary conditions $u_x = 0$, $u_z = 0$.

First, we study the results of a finite element computation of the original Scordelis-Lo roof on a reasonably fine mesh consisting of 20×20 MITC9 elements for the whole structure. Figure 4 shows that high stresses are present in the centre of the shell (corresponding to the bending moment), near the corners (corresponding to the in-plane shear stresses), and near

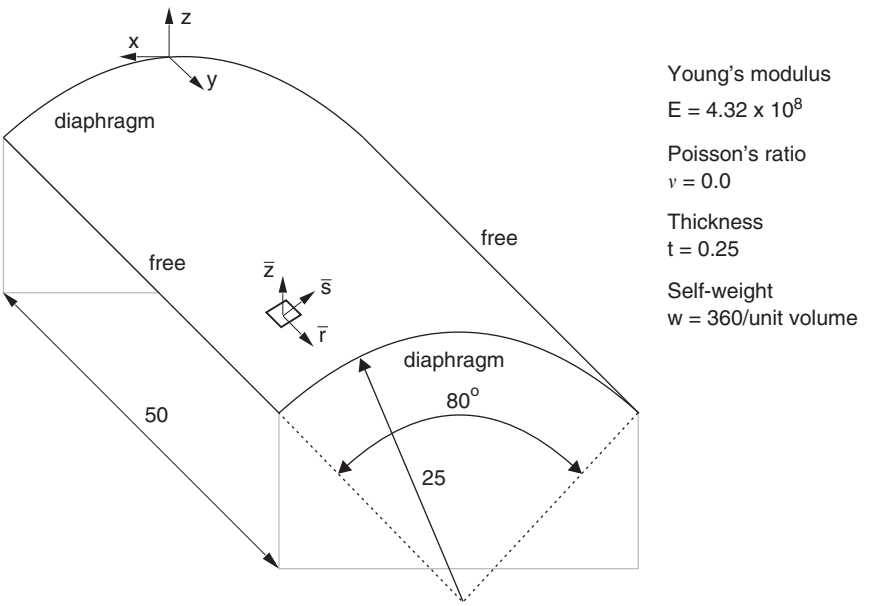

Figure 3. Scordelis-Lo roof.

the free boundaries (corresponding to the membrane stresses). Hence, we want to evaluate the following quantities of interest as also indicated in Figure 4(d):

$$Q_1(\mathbf{U}) = |\Omega_1|^{-1} \int_{\Omega_1} \bar{z}\sigma_{\bar{r}\bar{r}}(\mathbf{U})\,\mathrm{d}V \tag{78}$$

$$Q_2(\mathbf{U}) = |\Omega_2|^{-1} \int_{\Omega_2} \sigma_{\bar{r}\bar{s}}(\mathbf{U})\,\mathrm{d}V \tag{79}$$

$$Q_3(\mathbf{U}) = |\Omega_3|^{-1} \int_{\Omega_3} \sigma_{\bar{s}\bar{s}}(\mathbf{U})\,\mathrm{d}V \tag{80}$$

The reference solution was obtained using a uniform mesh of 200×200 MITC9 elements (with 802 401 degrees of freedom) for the complete structure. As seen in Figure 5 for every quantity of interest the estimated relative percentage error using the MITC4 element in the analysis decreases quickly and the corresponding effectivity indices are close to 1.0.

In our asymptotic study, we focus on the quantity of interest $Q_1(\mathbf{U})$ and we calculate the corresponding influence function for different shell thicknesses. As seen in Figure 6(a) the influence function corresponding to the original thickness, which is $\varepsilon = 10^{-2}$, is similar to the influence function of the bending moment of a simply supported beam. However, as the thickness tends to zero, we observe oscillations in the influence function and the local character of the influence function disappears while boundary layer effects become visible. This behaviour should be further studied in relation to the asymptotic analysis results published in Reference [29].

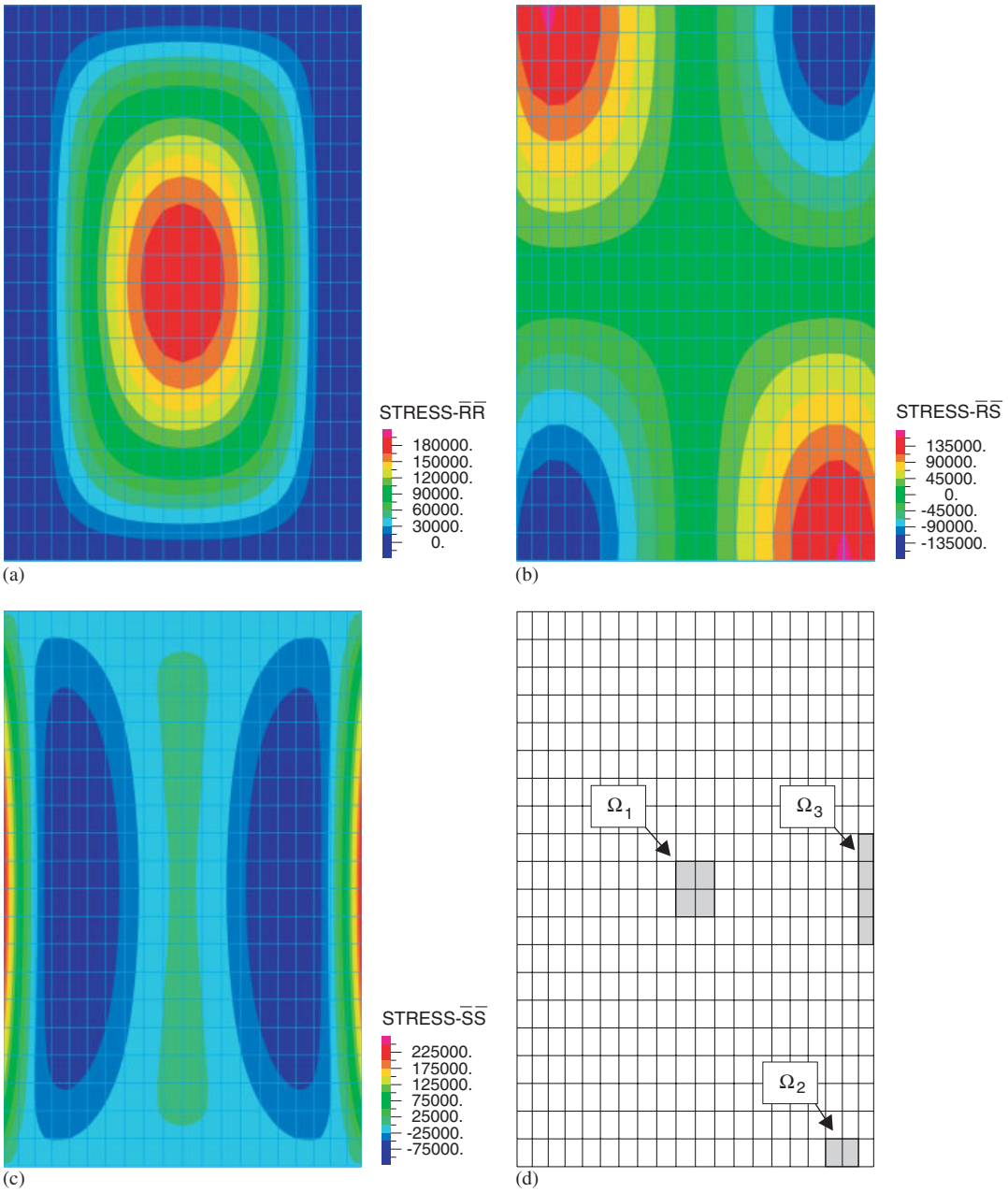

Figure 4. Stresses of the original Scordelis-Lo roof (top view) using a 20×20 MITC9 mesh: (a) $\sigma_{\bar{r}\bar{r}}$-stress field; (b) $\sigma_{\bar{r}\bar{s}}$-stress field; (c) $\sigma_{\bar{s}\bar{s}}$-stress field; and (d) locations of three quantities of interest.

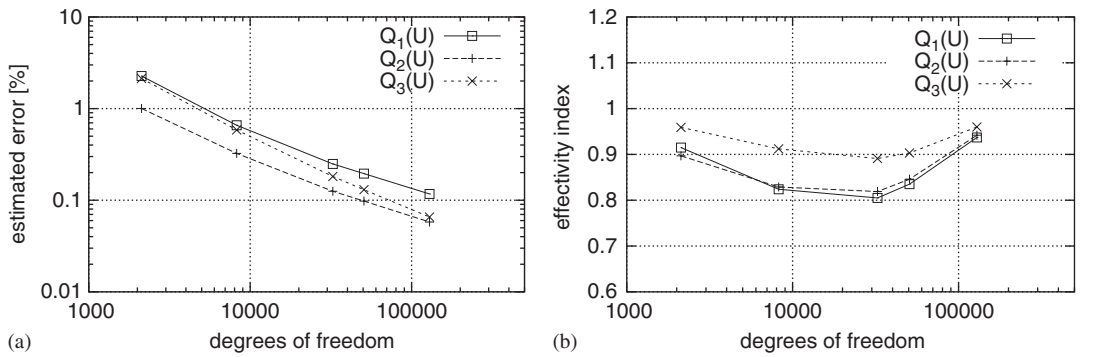

Figure 5. Results of goal-oriented error estimation for the original Scordelis-Lo roof for different quantities of interest: (a) estimated (absolute) relative errors in the quantities of interest; and (b) corresponding effectivity indices. The numbers of degrees of freedom refer to the uniform MITC4 element meshes used for the complete shell.

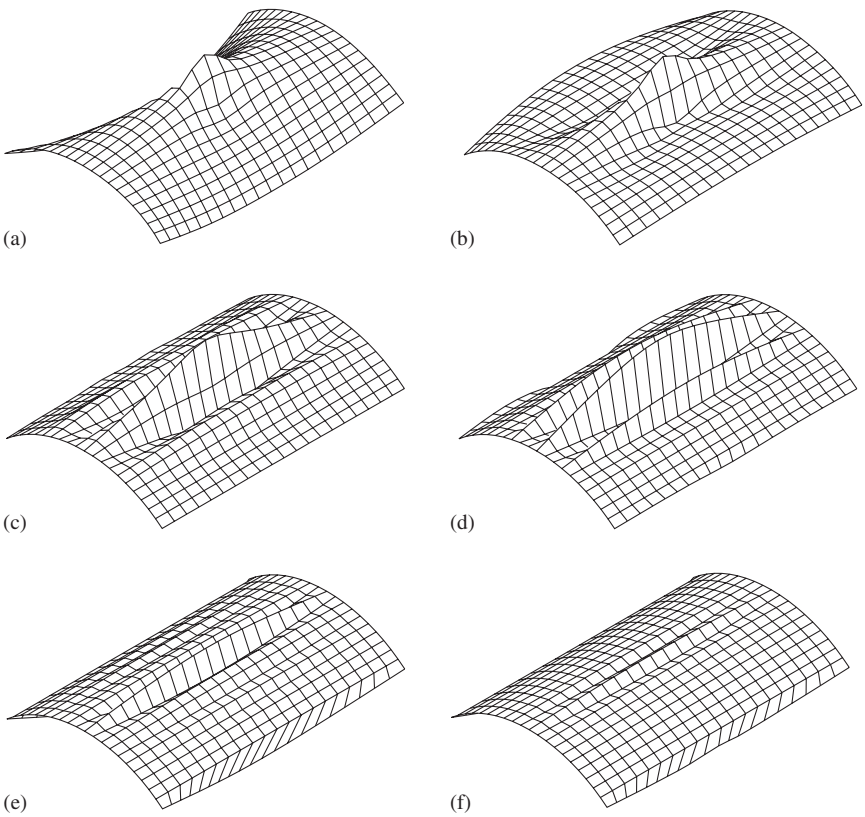

Figure 6. The influence function for the quantity of interest defined in (78) (integrated bending moment in the centre of the roof over four elements) for different shell thicknesses: (a) $\varepsilon = 10^{-2}$; (b) $\varepsilon = 10^{-3}$; (c) $\varepsilon = 10^{-4}$; (d) $\varepsilon = 10^{-5}$; (e) $\varepsilon = 10^{-6}$; and (f) $\varepsilon = 10^{-7}$.

6.3. Partly clamped hyperbolic parabolic shell problem

The partly clamped hyperbolic parabolic shell problem shown in Figure 7 is a bending dominated problem [2, 3]. The surface is defined by

$$\begin{pmatrix} x \\ y \\ z \end{pmatrix} = L \begin{pmatrix} \xi^1 \\ \xi^2 \\ (\xi^1)^2 - (\xi^2)^2 \end{pmatrix}, \quad (\xi^1, \xi^2) \in \left[-\frac{1}{2}, \frac{1}{2}\right]^2 \tag{81}$$

and is clamped along the side $y = -L/2$. We choose $L = 1$ and the vertical body load per unit volume is

$$\mathbf{F} = \begin{pmatrix} 0 \\ 0 \\ 100 \end{pmatrix} \tag{82}$$

A detailed finite element analysis of this shell problem shows high stresses in the areas indicated in Figure 8. Hence, we choose the following quantities of interest:

$$Q_1(\mathbf{U}) = |\Omega_1|^{-1} \int_{\Omega_1} \sigma_{\bar{r}\bar{r}}(\mathbf{U})\, \mathrm{d}V \tag{83}$$

$$Q_2(\mathbf{U}) = |\Omega_2|^{-1} \int_{\Omega_2} \sigma_{\bar{s}\bar{s}}(\mathbf{U})\, \mathrm{d}V \tag{84}$$

$$Q_3(\mathbf{U}) = |\Omega_3|^{-1} \int_{\Omega_3} \sigma_{\bar{r}\bar{r}}(\mathbf{U})\, \mathrm{d}V \tag{85}$$

$$Q_4(\mathbf{U}) = |\Omega_2|^{-1} \int_{\Omega_2} \bar{z}\, \sigma_{\bar{r}\bar{r}}(\mathbf{U})\, \mathrm{d}V \tag{86}$$

The reference fine mesh consists of 160×160 MITC9 elements (with 513 600 degrees of freedom) for the complete structure. Figure 9(a) shows the estimated relative errors in the quantities of interest, which reduce significantly with increasing numbers of degrees of freedom in the MITC4 element meshes. Although we focus on stresses that are difficult to solve for accurately, the effectivity indices are close to 1.0, see Figure 9(b).

We also want to study the error in the influence function itself since this error visualizes how elements contribute to the total error in the quantity of interest. Figure 10 displays the percentage value of the approximate error of the influence function corresponding to and normalized with the quantity of interest defined in (83), $(\hat{\mathbf{Z}}_h^{(M9)} - \hat{\mathbf{Z}}_h)/Q_1(\mathbf{U})$, using the 20×20 mesh. As expected, the error is not largest if the load acts in the area of interest but is larger when the load is at some distance. For instance, a vertical point load $F_3 = 1$ applied at the left tip would yield an error in the quantity of interest of about 49.5% and when applied at the right tip would yield an error of about -6.1% (see Figure 10(c)). It is also clear that contributions from loads in

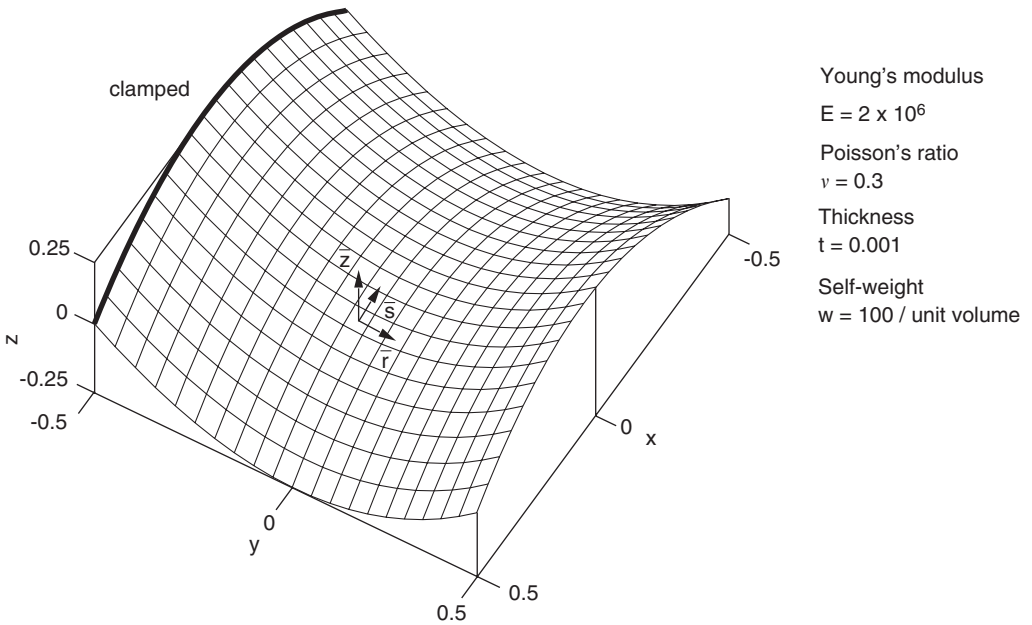

Figure 7. Partly clamped hyperbolic parabolic shell problem.

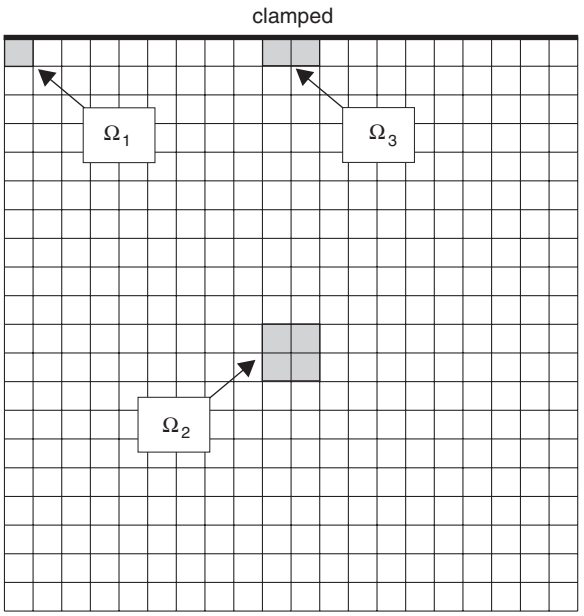

Figure 8. Partly clamped hyperbolic parabolic shell problem: locations of quantities of interest (top view). 20×20 mesh shown.

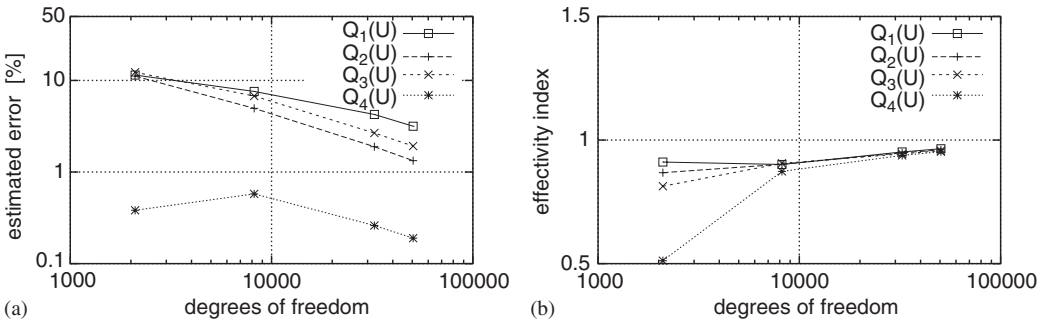

Figure 9. Results of goal-oriented error estimation for the hyperbolic parabolic shell problem for different meshes: (a) estimated (absolute) relative errors in the quantities of interest; and (b) corresponding effectivity indices. The numbers of degrees of freedom refer to the uniform MITC4 element meshes used for the complete shell.

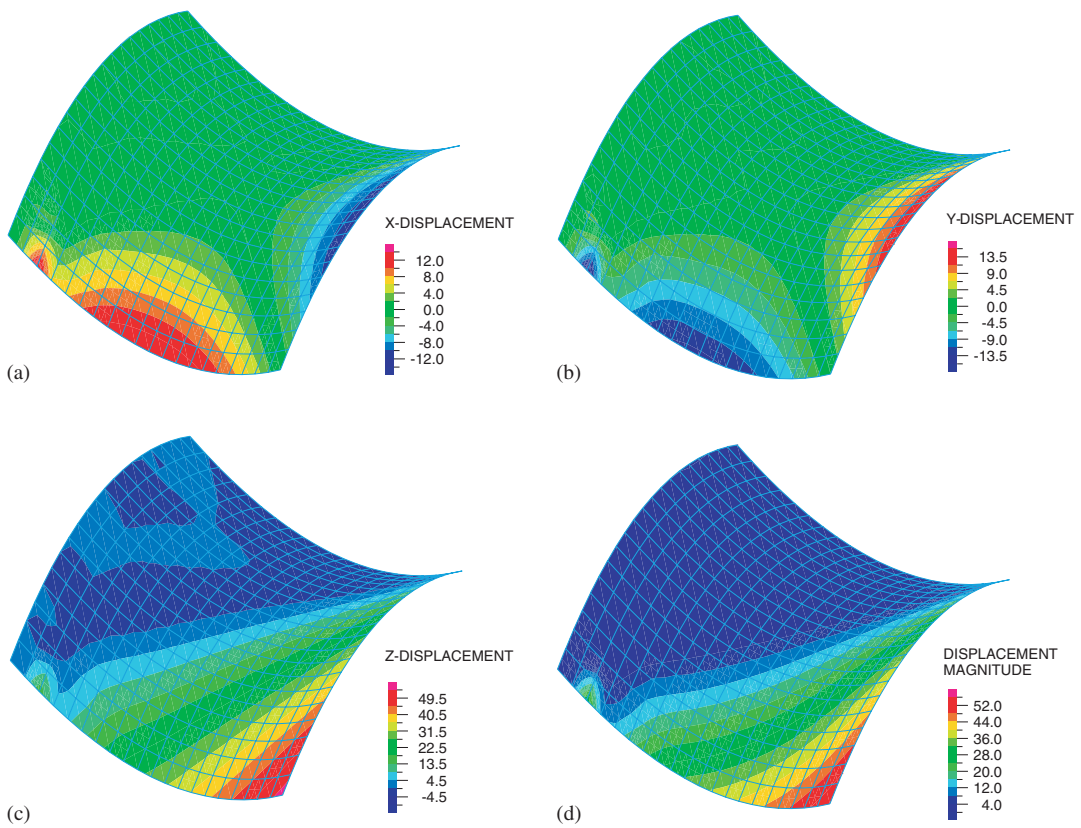

Figure 10. Approximate error of the influence function (percentage value) corresponding to and normalized with the quantity of interest defined in (83): (a) relative error corresponding to x direction; (b) relative error corresponding to y direction; (c) relative error corresponding to z direction; and (d) relative error in the displacement magnitude (Euclidean norm of the displacement vector).

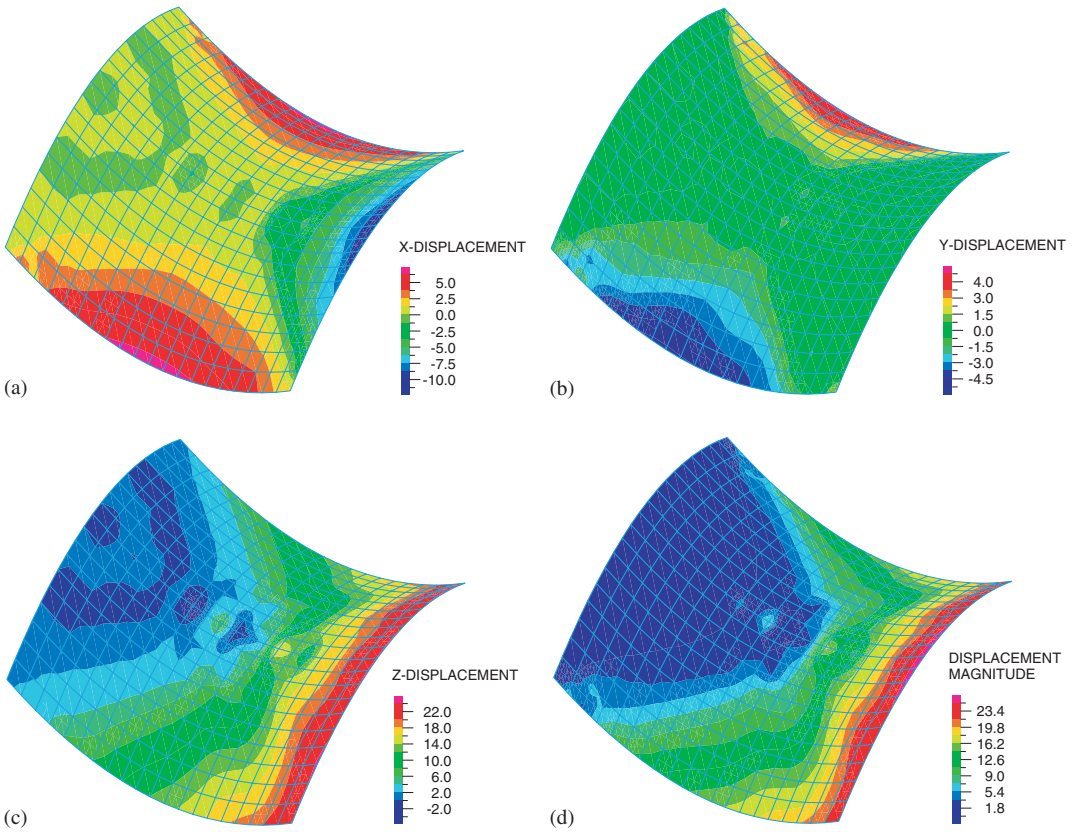

Figure 11. Approximate error of the influence function (percentage value) corresponding to and normalized with the quantity of interest defined in (84): (a) relative error corresponding to x direction; (b) relative error corresponding to y direction; (c) relative error corresponding to z direction; and (d) relative error in the displacement magnitude (Euclidean norm of the displacement vector).

the x and y directions are not negligible and may account for about one fourth of the error due to loads in the z direction.

It is important to emphasize that a proper consideration of the cancellation effect of the error over the analysis domain is essential for an efficient error estimate. For instance, assuming a constant body load in the y direction, the error is approximately zero because positive and negative contributions to the error are cancelled out. Hence, the application of any standard error estimator based on the energy norm results in a large over-estimation of the error. The reason is that in energy norm results only elementwise positive values contribute to the total error, while in our error estimate positive and negative values lead to the cancellation effect in the error estimation [17, 27, 28].

As another example, Figure 11 shows the error plot of the influence function for the quantity of interest defined in (84) and our remarks apply as well.

Figures 12 and 13 show again the pointwise accuracy of the influence function when using the 20×20 mesh for the quantity $Q_1(\mathbf{U})$ and we consider once more the value $(\hat{\mathbf{Z}}_h^{(M9)} - \hat{\mathbf{Z}}_h)/Q_1(\mathbf{U})$. However, in contrast to Figures 10 and 11, we define a tolerance on

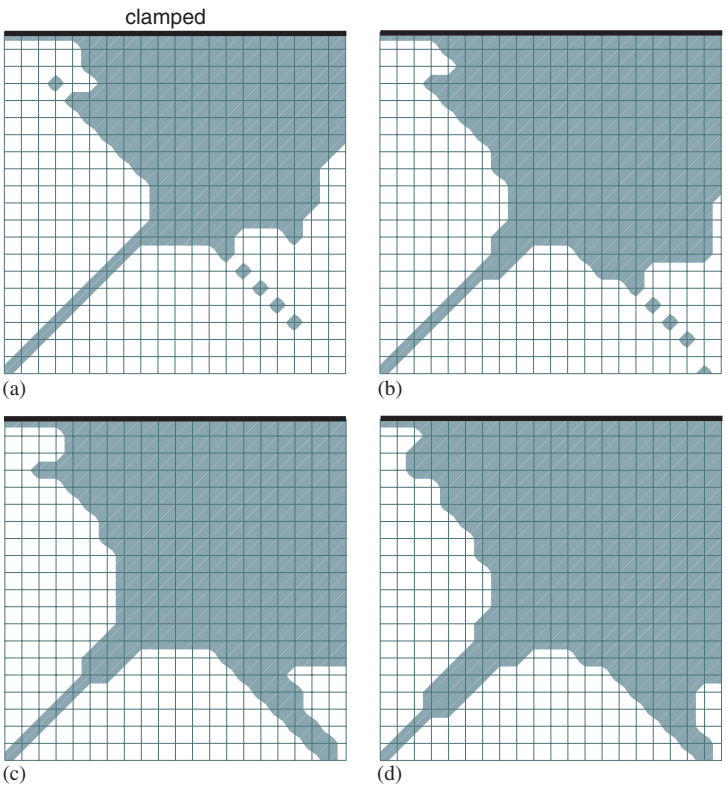

Figure 12. Predicted absolute pointwise accuracy of the influence function corresponding to and normalized with the quantity of interest defined in (83). Body loads in the y direction in the grey region yield an error in the quantity of interest smaller than a tolerance of: (a) tol = 0.5%; (b) tol = 1.0%; (c) tol = 1.5%; and (d) tol = 2.0%.

the absolute value, e.g. tol = 0.5%, and then the grey regions in Figures 12 and 13 indicate that the error is smaller than the tolerance if the load is applied there, while the white areas correspond to errors larger than the tolerance.

7. CONCLUSIONS

In this paper we proposed a consistent technique to calculate influence functions for arbitrary quantities of interest of shell structures. Using the influence functions, we can efficiently obtain the stresses in specific areas of interest when a large number of load cases must be considered.

We also discussed goal-oriented error measures and designed a measure for shell structural analysis when a shell mixed formulation is used. This error measure is simple to calculate and deemed quite effective because it includes the cancellation effect discussed in the paper. In the shell problems considered, accurate error predictions are achieved, even on coarse meshes and using uniformly refined meshes with the MITC4 and MITC9 shell elements. The corresponding

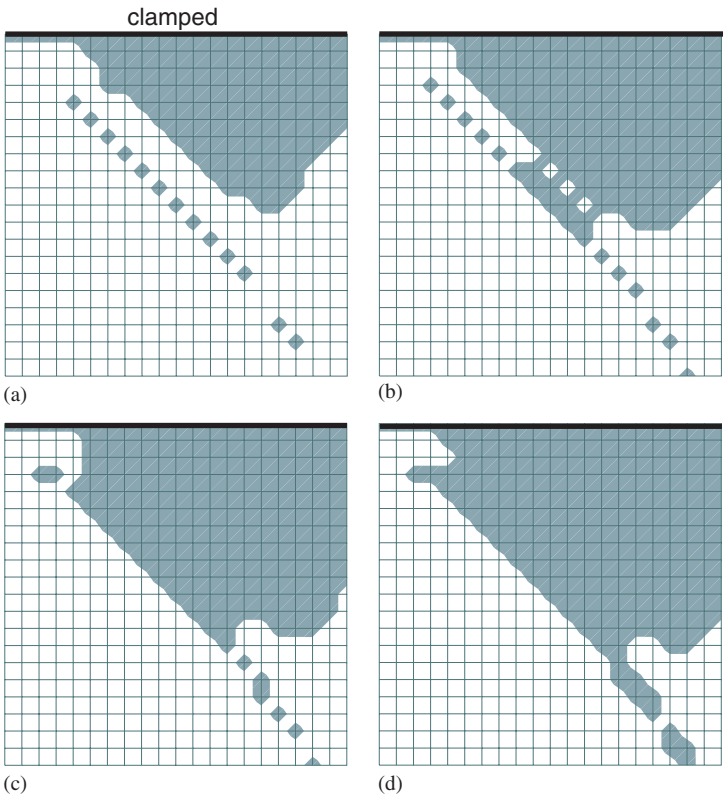

Figure 13. Predicted absolute pointwise accuracy of the influence function corresponding to and normalized with the quantity of interest defined in (83). Body loads in the z direction in the grey region yield an error in the quantity of interest smaller than a tolerance of: (a) tol = 0.5%; (b) tol = 1.0%; (c) tol = 1.5%; and (d) tol = 2.0%.

effectivity indices are close to 1.0 for the cases considered. The use of the procedures with other MITC shell elements, notably triangular elements [30], can be achieved directly, and the extension of the proposed goal-oriented error measure to non-linear shell problems and fluid flows with structural interactions is also possible [28].

ACKNOWLEDGEMENTS

The work of Thomas Grätsch was supported by the German Research Foundation (DFG) under contract GR 1894/2-1. We are grateful for this support.

REFERENCES

1. Bathe KJ (ed.). *Computational Fluid and Solid Mechanics*. Elsevier: Amsterdam, 2003.
2. Chapelle D, Bathe KJ. Fundamental considerations for the finite element analysis of shell structures. *Computers and Structures* 1998; **66**:19–36.
3. Chapelle D, Bathe KJ. *The Finite Element Analysis of Shells—Fundamentals*. Springer: Berlin, 2003.

4. Çirak F, Ramm E. *A posteriori* error estimation and adaptivity for linear elasticity using the reciprocal theorem. *Computer Methods in Applied Mechanics and Engineering* 1998; **156**:351–362.
5. Prudhomme S, Oden JT, Westermann T, Bass J, Botkin M. Practical methods for *a posteriori* error estimation in engineering applications. *International Journal for Numerical Methods in Engineering* 2003; **56**:1193–1224.
6. Oden JT, Prudhomme S, Westermann T, Bass J, Botkin M. Error estimation of eigenfrequencies for elasticity and shell problems. *Mathematical Models and Methods in Applied Sciences* 2003; **13**:323–344.
7. Bangerth W, Rannacher R. *Adaptive Finite Element Methods for Differential Equations*. Birkhäuser: Basel, 2003.
8. Becker R, Rannacher R. A feed-back approach to error control in finite element methods: basic analysis and examples. *East–West Journal of Numerical Mathematics* 1996; **4**:237–264.
9. Rannacher R, Suttmeier FT. A feed-back approach to error control in finite element methods: application to linear elasticity. *Computational Mechanics* 1997; **19**:434–446.
10. Bathe KJ. *Finite Element Procedures*. Prentice-Hall: Englewood Cliffs, NJ, 1996.
11. Hiller JF, Bathe KJ. Measuring convergence of mixed finite element discretizations: an application to shell structures. *Computers and Structures* 2003; **81**:639–654.
12. Chapelle D, Bathe KJ. The mathematical shell model underlying general shell elements. *International Journal for Numerical Methods in Engineering* 2000; **48**:289–313.
13. Bathe KJ, Iosilevich A, Chapelle D. An evaluation of the MITC shell elements. *Computers and Structures* 2000; **75**:1–30.
14. Dvorkin EN, Bathe KJ. A continuum mechanics based four-node shell element for general nonlinear analysis. *Engineering Computations* 1984; **1**:77–88.
15. Bucalem M, Bathe KJ. Higher-order MITC general shell elements. *International Journal for Numerical Methods in Engineering* 1993; **36**:3729–3754.
16. Bathe KJ, Lee PS, Hiller JF. Towards improving the MITC9 shell element. *Computers and Structures* 2003; **81**:1085–1097.
17. Babuška I, Strouboulis T. *The Finite Element Method and its Reliability.* Oxford Science Publications: Oxford, 2001.
18. Prudhomme S, Oden JT. On goal-oriented error estimation for elliptic problems: application to the control of pointwise errors. *Computer Methods in Applied Mechanics and Engineering* 1999; **176**:313–331.
19. Eriksson K, Estep D, Hansbo P, Johnson C. Introduction to adaptive methods for differential equations. *Acta Numerica* 1995; **4**:105–158.
20. Estep D. *A posteriori* error bounds and global error control for approximations of ordinary differential equations. *SIAM Journal on Numerical Analysis* 1995; **32**:1–48.
21. Grätsch T, Hartmann F. Finite element recovery techniques for local quantities of linear problems using fundamental solutions. *Computational Mechanics* 2003; **33**:15–21.
22. Oden JT, Prudhomme S. Goal-oriented error estimation and adaptivity for the finite element method. *Computers and Mathematics with Applications* 2001; **41**:735–756.
23. Paraschivoiu M, Peraire J, Patera A. *A posteriori* finite element bounds for linear-functional outputs of elliptic partial differential equations. *Computer Methods in Applied Mechanics and Engineering* 1997; **150**: 289–312.
24. Paraschivoiu M, Patera A. A hierarchical duality approach to bounds for the outputs of partial differential equations. *Computer Methods in Applied Mechanics and Engineering* 1998; **158**:389–407.
25. Huerta A, Rodriguez-Ferran A, Diez P, Sarrate J. Adaptive finite element strategies based on error assessment. *International Journal for Numerical Methods in Engineering* 1999; **46**:1803–1818.
26. Chapelle D, Bathe KJ. Optimal consistency errors for general shell elements. *Comptes Rendus de l'Académie des Sciences*. Série I—Mathématique, t. 332, 2001; 771–776.
27. Estep D, Holst M, Larson M. Generalized Green's functions and the effective domain of influence. *SIAM Journal on Scientific Computing*, to appear.
28. Grätsch T, Bathe KJ. *A posteriori* error estimation techniques in practical finite element analysis. *Computers and Structures* 2005; **83**:235–265.
29. Lee PS, Bathe KJ. On the asymptotic behavior of shell structures and the evaluation in finite element solution. *Computers and Structures* 2002; **80**:235–255.
30. Lee PS, Bathe KJ. Development of MITC isotropic triangular shell finite elements. *Computers and Structures* 2004; **82**:945–962.

